Thompson, C. L., Johnson, C. E., Dickson, D. P. E., Cammack, R., Hall, D. O., Weser, U., & Rao, K. K. (1974) *Biochem. J. 139*, 97-103.
Thorneley, R. N. F., Lowe, D. J., Eady, R. R., & Miller, R. W. (1979) *Biochem. Soc. Trans. 7*, 633-636.
Tsukihara, T., Fukuyama, K., Nakamura, T., Katsube, Y., Tanaka, N., Kukudo, Wada, M. K., Hase, T., & Matsubara, H. (1981) *J. Biochem. 90*, 1763-1773.
Walker, G., & Mortensen, L. E. (1973) *Biochem. Biophys. Res. Commun. 53*, 904-909.
Zumft, W. G., Palmer, G., & Mortenson, L. E. (1973) *Biochim. Biophys. Acta 292*, 413-421.
Zumft, W. G., Mortenson, L. E., & Palmer, G. (1974) *Eur. J. Biochem. 46*, 525-536.

Human Plasma Fibronectin Structure Probed by Steady-State Fluorescence Polarization: Evidence for a Rigid Oblate Structure†

Michael J. Benecky,* Carl G. Kolvenbach,‡ Richard W. Wine, James P. DiOrio, and Michael W. Mosesson

Sinai Samaritan Medical Center, University of Wisconsin Medical School, Milwaukee Clinical Campus, Milwaukee, Wisconsin 53233

Received September 29, 1989; Revised Manuscript Received November 20, 1989

ABSTRACT: In order to more clearly define the structure of human plasma fibronectin (PFn) under physiologic buffer conditions, we determined the mean harmonic rotational relaxation times (ρ_H) of PFn and the thrombin-derived 190/170-kDa PFn fragment using steady-state fluorescence polarization. These measurements utilized the long lifetime emission ($\tau = 1.2 \times 10^{-7}$ s) exhibited by 1-pyrenebutyrate, which had been covalently attached to amino groups at random sites on the PFn subunit. Our data analysis assumed that two independent processes depolarize the fluorescence exhibited by the dansylcadaverine and 1-pyrenebutyrate conjugates of PFn: (A) rapid ($\rho_H < 10^{-9}$ s) "thermally-activated" localized rotational motion of the protein side chains bearing the fluorescent probe [Weber, G. (1952) *Biochem. J. 51*, 145-154] and (B) slow ($\rho_H \sim 10^{-6}$ s) temperature-independent global rotational motion of the whole PFn molecule. Since only the ρ_H associated with the latter process is a true hydrodynamic parameter (i.e., sensitive to size and/or shape of the PFn molecule), we utilized isothermal polarization measurements to discriminate against the interfering signal arising from "thermally activated" probe rotation. The ρ_H (4.4 ± 0.9 μs) derived from an experiment in which pyrene–PFn fluorescence polarization was monitored as a function of sucrose concentration at constant temperature is 7 (±1.4) times longer than that predicted for an equivalent hydrated sphere. We propose that "thermally activated" probe rotation gives rise to the nearly 100-fold shorter PFn ρ_H values previously reported in the literature. Consequently, our data exclude all previous models which invoke segmental flexibility of the PFn peptide backbone. The simplest hydrodynamic model supported by our fluorescence data is an oblate ellipsoid with an axial ratio of 15:1. All prolate models can be unambiguously excluded by this result. We estimate that the disk-shaped PFn molecule has a diameter and thickness of 30 and 2 nm, respectively. Electron microscopy of negatively stained PFn specimens on carbon also showed PFn to have a compact rounded structure. The much faster rotational relaxation rate of the pyrene–190/170-kDa PFn fragment ($\rho_H = 0.92 \pm 0.11$ μs) compared to pyrene–PFn indicated that this monomeric PFn fragment, like native PFn, had an oblate shape under physiologic buffer conditions.

Plasma fibronectin (PFn)[1] is a 520-kDa (Rocco et al. 1987; Sjöberg et al., 1987) heterodimeric glycoprotein which mediates cell attachment and spreading in a wide variety of biological systems. The molecular basis for this adhesive biological activity resides in its multiple binding affinities for various macromolecules found within cells, on cell surfaces, and in extracellular matrices. Although PFn has been characterized by a wide variety of biophysical techniques [for reviews, see Hermans (1985) and Odermatt and Engel (1989)], the relationship between PFn structure and its various adhesive biological functions remains poorly understood. Furthermore, these previous biophysical studies have not yet

† This investigation was supported by NHLBI Program Project Grant HL-28444. An abstract of this work was presented at the American Society for Cell Biology and the American Society for Biochemistry and Molecular Biology Joint Meeting, January 29–February 2, 1989, San Francisco, CA (Benecky et al., 1988b).

* Address correspondence to this author at the Sinai Samaritan Medical Center, Winter Research Institute, 836 North Twelfth St., Milwaukee, WI 53233.

‡ Present address: Amgen Corp., 1900 Oak Terrace Lane, Thousand Oaks, CA 91320.

[1] Abbreviations: PFn, human plasma fibronectin; ρ_H, mean harmonic rotational relaxation time; TBS, Tris-buffered saline (50 mM Tris-HCl/150 mM NaCl, pH 7.4, buffer); EDTA, ethylenediaminetetraacetic acid; PMSF, phenylmethanesulfonyl fluoride; KIU, kallikrein inactivator unit(s); SDS, sodium dodecyl sulfate; SDS–PAGE, sodium dodecyl sulfate–polyacrylamide gel electrophoresis, τ, fluorescence lifetime; PBS, phosphate-buffered saline (30 mM sodium phosphate/100 mM NaCl, pH 7.4, buffer); $\langle\tau\rangle$, second-order average fluorescence lifetime; η, solvent viscosity; ρ_o, rotational relaxation time expected for an equivalent hydrated sphere; pyrene–PFn, 1-pyrenebutyrate-conjugated PFn; CD, circular dichroism; STEM, scanning transmission electron microscopy; ANS–PFn, 1-anilino-8-naphthalenesulfonate-conjugated PFn.

0006-2960/90/0429-3082$02.50/0

clearly elucidated the solution structure of the PFn molecule under physiologic buffer conditions.

Electron microscopy of PFn that had been rotary-shadowed onto mica from glycerol-containing buffers of physiologic ionic strength revealed slender "strand-like structures" characterized by contour lengths in the 120–160-nm range (Engel et al., 1981; Erickson et al., 1981). A wide assortment of more compact structures (with dimensions ranging from 15 × 9 nm to 50 × 30 nm) have been reported in electron microscopic investigations of PFn that had been rotary-shadowed from a low ionic strength buffer (Erickson & Carrell, 1983) or deposited upon thin carbon films (Koteliansky et al., 1980; Price et al., 1982; Tooney et al., 1983). Sedimentation velocity measurements indicate that the PFn molecule deviates significantly from spherical symmetry, since the observed $s_{20,w}$ (13 S) (Mosesson & Umfleet, 1970) is much slower than that predicted for a sphere (21 S) (Odermatt et al., 1982). More recently, Sjöberg et al. (1987) have employed small-angle X-ray and neutron scattering to study PFn structure at physiological pH and ionic strength. The hydrodynamic model which best fit this data was an oblate ellipsoid (i.e., disk) having a diameter and thickness of 27.6 and 2.88 nm, respectively.

Previous studies which have utilized nonisothermal fluorescence polarization measurements to study the rotational diffusion of PFn (Williams et al., 1982) or PFn fragments (Forastieri & Ingham, 1985) have yielded rotational relaxation times 1–2 orders of magnitude shorter than that predicted by a rigid spherical model. Similar results were obtained when the rotational relaxation time of PFn was estimated from electron spin resonance measurements (Lai & Tooney, 1984; Lai et al., 1984; Narasimhan & Lai, 1989). All of the above observations have been taken as supporting evidence for PFn segmental flexibility, i.e., a structure in which the constituent domains of the molecule can rotate independently of each other.

In order to more clearly define PFn structure under physiologic buffer conditions, we determined the rotational relaxation times of PFn and the monomeric thrombin-derived 190/170-kDa PFn fragment using steady-state fluorescence polarization. This study employed the long lifetime emission exhibited by an extrinsic fluorophore, 1-pyrenebutyrate, which had been covalently attached to amino groups at random sites on the PFn subunit. We calculated the rotational relaxation time (ρ_H) from fluorescence polarization measurements obtained as a function of the temperature to solvent viscosity ratio (Weber, 1953). Our data analysis assumed that two independent processes account for all the observed depolarization: (A) rapid (subnanosecond) "thermally-activated" localized rotational motion of the protein side chains bearing the fluorescent probe (Weber, 1952) and (B) slow (microsecond) temperature-independent global rotation of the whole PFn molecule. Only the ρ_H associated with the latter process is a hydrodynamic parameter which reflects the size and shape of the PFn molecule. We show that the large depolarization observed when the sample is heated emanates from the "thermally-activated" rotational motion of the fluorescent probe. Consequently, the shorter than expected ρ_H values derived from previous nonisothermal polarization measurements (Williams et al., 1982; Forastieri & Ingham, 1985; Ingham et al., 1988) are not a valid representation of the hydrodynamic properties of the PFn molecule. When isothermal conditions were used to discriminate against the depolarization originating from "thermally-activated" probe rotation, we found that fluorescence polarization showed PFn to be a rigid, disk-shaped molecule. This observation forms the basis for this report.

Materials and Methods

Outdated human plasma was obtained from the Blood Center of Southeastern Wisconsin (Milwaukee, WI). We purchased 5-aminopentyl-(dimethylamino)-1-naphthalenesulfonamide (dansylcadaverine) and succinimidyl 1-pyrenebutyrate [10% (w/w) adsorbed on Celite] from Molecular Probes (Eugene, OR). α-Thrombin and factor XIII were generous gifts from Drs. John Fenton (New York State Department of Health, Albany, NY) and Kevin Siebenlist (Sinai Samaritan Medical Center, Milwaukee, WI), respectively. The isolation of factor XIII from human plasma followed a published method (Lorand & Gotoh, 1970). Sepharose 4B-CL and trasylol were from Pharmacia (Piscataway, NJ) and Mobay Chemical Corp. (New York, NY), respectively. Heparin- and gelatin–Sepharose 4B-CL affinity resins were prepared by a modification (Homandberg et al., 1985) of a previously described method (March et al., 1974).

Isolation and Characterization of PFn and the Thrombin-Derived 190/170-kDa PFn Fragment. We isolated PFn from outdated human plasma employing gelatin–Sepharose affinity chromatography with 50 mM sodium citrate–150 mM NaCl, pH 5.5, elution (Miekka et al., 1982; Smith & Griffin, 1985). For certain preparations of PFn, we employed gelatin–Sepharose chromatography using 3 M urea–TBS elution (Engvall & Ruoslahti, 1977). PFn was quantitated from its absorbance at 280 nm using its known extinction coefficient [ϵ = 1.28 cm^2mg^{-1} (Mosesson & Umfleet, 1970)]. PFn-containing fractions (>1 mg/mL) from the gelatin–Sepharose column were pooled, dialyzed extensively against TBS, stored at 4 °C, and used within 2 weeks of isolation. During isolation and storage, all buffers and PFn stock solutions contained 0.5 mM EDTA, 0.10 mM PMSF, 0.02% (w/v) sodium azide, and 1 KIU/mL trasylol. Upon SDS–PAGE (Laemmli, 1970) of reduced specimens on 5% polyacrylamide gels, PFn migrated as a closely spaced doublet at 220–225 kDa. SDS–PAGE under nonreducing conditions confirmed that >85% of the total protein migrated as the 450-kDa dimer with the remainder migrating in the position of the 235-kDa PFn component (Chen et al., 1977).

Conditions for the digestion of PFn by thrombin (Homandberg & Erickson, 1986) and cathepsin D (Balian et al., 1979) have been reported previously. The preparation and characterization of the thrombin-derived 190/170-kDa and 29-kDa PFn fragments have been described previously (Homandberg & Erickson, 1986; Benecky et al., 1988a). The 190/170-kDa PFn fragment was quantitated from its absorbance at 280 nm using ϵ = 1.20 cm^2 mg^{-1} (Homandberg & Erickson, 1986). The amino acid sequence of this fragment began at position 260 (Homandberg & Erickson, 1986) in the PFn sequence (Kornblihtt et al., 1985). This indicated that the 190/170-kDa PFn fragment lacked the 30-kDa amino-terminal domain.

Preparation and Characterization of Dansylcadaverine–PFn. We employed factor XIIIa mediated cross-linking to label PFn covalently with dansylcadaverine (Williams et al., 1982). After a 2-h reaction period, gelatin–Sepharose chromatography with 3 M urea–TBS elution was used to separate dansylcadaverine–PFn from unreacted dansylcadaverine. The extent of label incorporation was quantified by comparing the fluorescence intensity (λ_{ex} = 350 nm; λ_{em} = 520 nm) of dansylcadaverine–PFn in 1% SDS at pH 7.4 to that of a known concentration of free dansylcadaverine in the same solvent (Williams et al., 1982). Typically, our dansylcadaverine–PFn

preparations contained 2 mol of dansylcadaverine/mol of PFn. Williams et al. (1982) have shown under these conditions labeling is confined to a single site (glutamine-3) near the amino terminus of each PFn subunit. The fluorescence lifetime ($\tau = 1.2 \times 10^{-8}$ s) of dansylcadaverine–PFn has been reported previously (Williams et al., 1982).

Preparation and Characterization of the 1-Pyrenebutyrate Conjugates of PFn and the 190/170-kDa PFn Fragment. PFn (0.80 mg/mL) was dialyzed against 50 mM $NaHCO_3$–100 mM NaCl, pH 8.5, buffer and then incubated with 1 mg/mL succinimidyl 1-pyrenebutyrate [10% (w/w) adsorbed on Celite]. We kept the Celite-adsorbed reagent in suspension during the reaction period through repeated inversion of the reaction vessel. After 45 min, the pH of the reaction mixture was adjusted to pH 7.4 by the addition of 0.10 M HCl, and the sample was then applied to a gelatin–Sepharose column (2-mL bed volume/mg of PFn applied). After extensive washing of the affinity resin with TBS, we eluted pyrene–PFn with 50 mM sodium citrate–150 mM NaCl, pH 5.5, buffer. Protein-containing fractions (>1 mg/mL) were pooled, dialyzed against TBS, and stored at 4 °C until use. The number of dye molecules bound per PFn molecule was determined by absorption spectroscopy using a molar extinction coefficient of 4.0×10^4 M^{-1} cm^{-1} at 346 nm for protein-bound 1-pyrenebutyrate (Knopp & Weber, 1969). We prepared the 1-pyrenebutyrate conjugate of the thrombin-derived 190/170-kDa PFn fragment in a similar manner, except that gelatin–Sepharose chromatography with 3 M urea–TBS elution was employed.

Absorption Spectra. UV/visible absorption spectra were recorded on a Gilford Response spectrophotometer using quartz cuvettes of 1-cm path length.

Fluorescence Emission Spectra. Fluorescence data were obtained on an SLM-Aminco SPF500C spectrofluorometer equipped with the manufacturer's polarization accessory. Pyrene–PFn emission spectra were obtained using 330-nm excitation with both excitation and emission polarizers in the vertical position. The slits for the emission and excitation ports were adjusted to yield a 5-nm band-pass. Pyrene–PFn samples were at 0.2 mg/mL in PBS. The solvent background was subtracted from the pyrene–PFn fluorescence data, but the data were left uncorrected for the wavelength-dependent response of the photomultiplier.

Gelatin- and Heparin–Sepharose Affinity Chromatography. We compared the affinities of pyrene–PFn and native PFn for gelatin–Sepharose in the following way. PFn (5 mg) was applied to a gelatin–Sepharose column (1 × 15 cm) that had been previously equilibrated in TBS. We washed the column with 50 mL of TBS and then eluted the bound PFn with a linear urea gradient (50 mL of TBS vs 50 mL of TBS–8 M urea) while collecting 1-mL fractions. We also compared the affinities of pyrene–PFn and native PFn for heparin–Sepharose. In this type of experiment, we dialyzed our samples (5 mg) against 20 mM Tris-HCl–50 mM NaCl, pH 7.4, buffer and then applied them to a heparin–Sepharose column (1 × 15 cm) which had been equilibrated in the same buffer. After the column was washed with 50 mL of the 20 mM Tris buffer containing 50 mM NaCl, bound PFn was eluted with a 100-mL linear salt gradient (50 mM NaCl vs 800 mM NaCl) while collecting 1-mL fractions.

Analytical Ultracentrifugation. Sedimentation velocity measurements in PBS were performed at 20 °C in a Beckman Model E analytical ultracentrifuge equipped with a photoelectric UV scanner. Centrifugation runs were at 56 000 rpm. Samples were adjusted to give an A_{280nm} reading of 0.80.

Far-UV Circular Dichroism. CD spectra were recorded on a JASCO J500A spectropolarimeter. PFn samples (0.5 mg/mL) subjected to CD analysis were dialyzed against 50 mM sodium phosphate, pH 7.4, buffer and then transferred to 0.2-mm path-length cylindrical quartz cells. We averaged four scans that were each accumulated between 255 and 185 nm in 0.2-nm increments, employing a scan speed of 5 nm/min, a gain of 10 mdeg/full scale, and a time constant of 4 s. The solvent background obtained under the identical experimental conditions was subtracted from the raw CD data. Conversion of the PFn CD data to mean residue ellipticity assumed a mean residue molecular weight of 108. We analyzed these data in terms of protein secondary structure elements using CONTIN (Provencher & Glöckner, 1981) on a Digital Equipment Corp. VAX computer at Marquette University (Milwaukee, WI). CD data for the thrombin-derived 190/170- and 29-kDa PFn fragments were obtained and analyzed in a similar manner.

Phase-Modulation Measurements of Pyrene–PFn Fluorescence Lifetime. We measured the pyrene–PFn fluorescence lifetime using the phase-modulation technique (Lakowicz, 1983a). These measurements were made on an SLM 48000S multiple-frequency phase-modulation spectrofluorometer at SLM Instruments, Inc., in Urbana, IL. Glycogen was employed as the zero lifetime standard. The exciting light ($\lambda = 330$ nm) passed through a 2-nm band-pass slit, and we employed an optical cutoff filter to collect all emission having $\lambda > 370$ nm. Pyrene–PFn samples were at 1 mg/mL in PBS. The temperature of the sample was maintained within ±0.2 °C of the desired temperature using a jacketted cell holder and a circulating water bath. For each sample, we measured the phase shift and demodulation of pyrene–PFn fluorescence as a function of modulation frequency between 0.8 and 3.0 MHz. We calculated the fluorescence lifetime(s) of pyrene–PFn from these data using an analysis previously outlined by Weber (1981). We performed these computations on an IBM PS/2 computer utilizing the software package that accompanied the SLM 48000S spectrofluorometer. In the case of doubly exponential fluorescence decay, we employed the second-order average lifetime, $\langle\tau\rangle = (\alpha_1^2\tau_1^2 + \alpha_2^2\tau_2^2)/(\alpha_1\tau_1 + \alpha_2\tau_2)$, in subsequent calculations of ρ_H (Brochon & Wahl, 1972). In this equation, α and τ denote each component's fractional contribution and fluorescence lifetime, respectively.

Fluorescence Polarization Measurements on the Dansylcadaverine and 1-Pyrenebutyrate Conjugates of PFn. We calculated the fluorescence polarization, P, using the single-channel method (Lakowicz, 1983b):

$$P = \frac{(I_{VV} - B_{VV}) - G(I_{VH} - B_{VH})}{(I_{VV} - B_{VV}) + G(I_{VH} - B_{VH})} \quad (1)$$

where $G = I_{HV}/I_{HH}$. I is the observed fluorescence intensity when the excitation (first subscript) and emission (second subscript) polarizers were in the vertical (V) and horizontal (H) positions, respectively. B is the emission intensity of a blank containing the same amount of underivatized PFn under identical experimental conditions. G is an instrument correction factor which accounts for the different transmission efficiency of the emission monochromator for vertically and horizontally polarized light. We monitored dansylcadaverine–PFn emission at 520 nm using 350-nm excitation. For pyrene–PFn, the excitation and emission wavelengths were 330 and 398 nm, respectively. The excitation and emission slits were both adjusted to yield a 7.5-nm band-pass. PFn samples were at 0.20 mg/mL in PBS. Each fluorescence

intensity determination was performed on duplicate samples, with a single measurement representing an average of 160 independent readings. The resulting polarization values were reproducible to within ±0.001. Sample temperature was thermostated to within ±0.10 °C of the desired temperature by using a circulating water bath and a jacketted cell holder.

Analysis of the Fluorescence Polarization Data Using the Perrin Equation. The fluorescence polarization exhibited by the dansylcadaverine and 1-pyrenebutyrate conjugates of PFn is expected to obey the following relationship (Perrin, 1934):

$$(1/P - 1/3) = (1/P_0 - 1/3)[1 + \beta(T/\eta)] \quad (2)$$

where $\beta = R\tau/V$. Therefore, a plot of $(1/P - 1/3)$ vs the temperature to solvent viscosity ratio (T/η) yields a line with slope $\beta(1/P_0 - 1/3)$ and intercept $(1/P_0 - 1/3)$. P_0 is the observed polarization in the absence of all molecular motion (i.e., $T/\eta = 0$). β is the ratio of the slope to the intercept of the Perrin plot, R is the gas constant, τ is the fluorescence lifetime, and V is the molecular volume. We can then calculate the rotational relaxation time, ρ, provided τ is known:

$$\rho = (3\tau/\beta)(T/\eta)^{-1} \quad (3)$$

This calculation assumed the solvent to be water at 25 °C ($T/\eta = 3.34 \times 10^4$ K P^{-1}). This equation can only be applied rigorously to spherical molecules (Perrin, 1934). However, Weber (1953) has extended this treatment to include elliptical macromolecules. In this case, the measured rotational relaxation time corresponds to ρ_H, the harmonic mean of the rotational relaxation times about the principal axes of the ellipsoid.

Perrin plots were constructed from polarization data obtained as a function of either temperature or sucrose concentration [0–55% (w/v)] at constant temperature. These analyses utilized previously tabulated viscosity data (Sober, 1970; Weast, 1972) and ignored the small increment in viscosity produced by the buffer salts (i.e., 30 mM sodium phosphate and 100 mM NaCl). P_0 was determined from the intercept of the nonisothermal Perrin plot. However, estimation of P_0 from polarization measurements made in highly viscous solvents (e.g., 55% sucrose at 4 °C) yielded similar results.

"Thermally Activated" Depolarization Arising from the Rotational Motion of the Fluorescent Probe. If rapid localized rotational motion of the fluorescent probe makes a contribution to the observed depolarization that is independent of the depolarization arising from the slow overall rotation of the macromolecule, a modified form of the Perrin equation must be employed in the analysis of the fluorescence polarization data (Wahl & Weber, 1967; Weltman & Edelman, 1967):

$$(1/P - 1/3) = (1/P_{0,app} - 1/3)[1 + \beta(T/\eta)] \quad (4)$$

where $(1/P_{0,app} - 1/3) = (1/[1 - f_2(T)])(1/P_0 - 1/3)$. $f_2(T)$, the fraction of the total fluorescence intensity arising from the rapidly rotating fluorescent probe, increases in its relative proportion at higher sample temperatures. $(1/P_{0,app} - 1/3)$ is the intercept of a Perrin plot derived from an experiment in which solvent viscosity was varied by the addition of sucrose at constant temperature [i.e., conditions where $f_2(T)$ is constant]. $(1/P_{0,app} - 1/3)$ will be larger than $(1/P_0 - 1/3)$ when depolarization due to probe rotation is operative. Equation 4 indicates that ρ_H can be determined from the low-viscosity component (i.e., ≤30% sucrose at 20 °C; $T/\eta > 8000$ K P^{-1}) of the isothermal Perrin plot, since this depolarization is derived exclusively from the slow overall rotation of the dimeric PFn molecule. Downward curvature in the isothermal Perrin plot observed at high viscosity (i.e., >40% sucrose; $T/\eta < 5000$ K P^{-1}) originates from the rapid localized rotational motion of the protein side chains bearing the fluorescent probe. The thermodynamic barrier to free rotation of the fluorescent probe was estimated from the temperature-dependent variation in $(1/P_{0,app} - 1/3)$ (Rawitch et al., 1969):

$$\ln (1/P_{0,app} - 1/3) = \text{constant} + (E_a/R)(1/T) \quad (5)$$

Thus, a plot of $\ln (1/P_{0,app} - 1/3)$ vs the reciprocal of the absolute temperature (in K^{-1}) will yield a line with slope E_a/R, where E_a is the "activation energy" for free probe rotation.

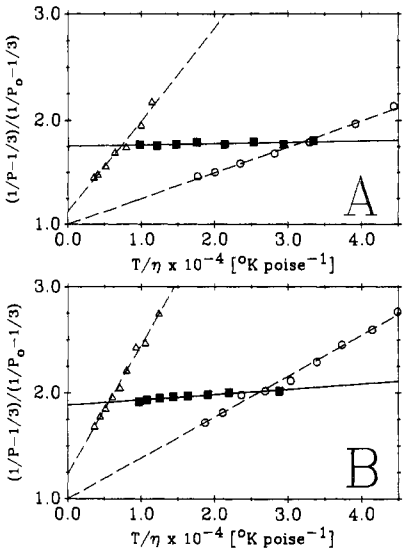

FIGURE 1: Perrin plots obtained by monitoring (A) dansylcadaverine–PFn and (B) pyrene–PFn fluorescence polarization in PBS as a function of either sucrose concentration [0–30% (w/v)] under isothermal conditions (■) or temperature (0–40 °C) in the presence (△) and absence (○) of 35% (w/v) sucrose. The isothermal Perrin plots for dansylcadaverine–PFn and pyrene–PFn were obtained at 25 and 20 °C, respectively. To facilitate the direct comparison of the dansylcadaverine–PFn and pyrene–PFn data, we have normalized the polarization data with respect to the limiting polarization, P_0. Therefore, $(1/P - 1/3)/(1/P_0 - 1/3) = 1$ denotes the absence of all molecular rotational motion. From the intercepts of the respective nonisothermal Perrin plots, we estimated the P_0 values of dansylcadaverine–PFn and pyrene–PFn to be 0.404 and 0.158, respectively.

Electron Microscopy. Transmission electron microscopy was carried out in a Philips 400T electron microscope at 60–80 kV. Ultrathin carbon films (25–30 Å in thickness) were prepared by a previously reported method (Wall et al., 1985). For negative staining, PFn (5.0 μg/mL in TBS) was deposited upon a wet carbon film and stained with 2% uranyl acetate. PFn samples for rotary-shadowing were dialyzed against a 0.15 M ammonium acetate, pH 7, buffer containing 30% (v/v) glycerol, diluted to a final concentration of 30 μg/mL, sprayed onto the carbon film, and rotary-shadowed with 25–30 Å of platinum at a shadowing angle of 7°.

Results

Rotational Relaxation Measurements on Dansylcadaverine–PFn. The mean harmonic rotational relaxation time (ρ_H) derived from an experiment in which dansylcadaverine–PFn fluorescence polarization was measured as a function of temperature (Figure 1A, circles) is much shorter ($\sim 5.0 \times 10^{-8}$ s) than that predicted by a spherical model ($\rho_0 = 6.28 \times 10^{-7}$ s). This is essentially a confirmation of an earlier observation (Williams et al., 1982). However, the Perrin plot derived from an experiment in which solvent viscosity was varied by the addition of sucrose at constant temperature (25 °C) exhibited negligible slope (Figure 1A,

squares). We estimate from these data that ρ_H is on the microsecond time scale.

The much shorter rotational relaxation time observed under nonisothermal conditions can be explained if we assume that both fast ($\rho_H < 10^{-9}$ s) localized rotational motion of the covalently attached dansylcadaverine probe and slow ($\rho_H \sim 10^{-6}$ s) overall rotation of the dimeric PFn molecule make independent contributions to the observed depolarization. This analysis, first developed by Weber (1952), predicts that probe rotation is "thermally activated" (i.e., its contribution to the observed depolarization increases at higher temperatures). The much shorter ρ_H observed under nonisothermal conditions (Figure 1A, circles) reflects "averaging" of the slow rotational motion of the protein ($\rho_H \sim 10^{-6}$ s) with the temperature-dependent fast rotational motion of the fluorescent probe ($\rho_H < 5.0 \times 10^{-8}$ s). We estimated the respective contribution of probe rotation to the observed depolarization (43% at 25 °C) from the intercepts of the nonisothermal and isothermal dansylcadaverine–PFn Perrin plots (Figure 1A) using eq 4. We also observed that ρ_H decreased significantly when the nonisothermal experiment was carried out in PBS containing 35% (w/v) sucrose (Figure 1A, triangles). The apparent decrease in ρ_H induced by 35% sucrose reflects the slow overall rotational motion of the protein being frozen while the fluorescent probe continues to exhibit unhindered rotation (Weltman & Edelman, 1967). The negligible slope associated with the isothermal dansylcadaverine–PFn Perrin plot (Figure 1A squares) implies that the PFn molecule does not exhibit significant rotational displacement during the lifetime of dansylcadaverine–PFn fluorescence (1.2×10^{-8} s). Depolarization originating from thermally activated probe rotation has been used to explain similar observations in fluorescence polarization investigations of rabbit γ-globulin (Wahl & Weber, 1967), human γG-immunoglobulins (Weltman & Edelman, 1967), thyroglobulin (Rawitch et al., 1969), and fibrinogen (Acuña et al., 1987).

Characterization of the 1-Pyrenebutyrate Conjugate of PFn. It became apparent that the relatively short fluorescent lifetime of the dansylcadaverine probe (1.2×10^{-8} s) made it insensitive to the slow overall rotation of the dimeric PFn molecule ($\rho_H \sim 10^{-6}$ s). In order to estimate ρ_H more precisely, we prepared the 1-pyrenebutyrate conjugate of PFn (pyrene–PFn) by the use of the amine reactive reagent succinimidyl 1-pyrenebutyrate. The longer fluorescence lifetime exhibited by 1-pyrenebutyrate ($\sim 10^{-7}$ s) makes this probe more sensitive to the slow rotational diffusion exhibited by large (>200 kDa) proteins (Knopp & Weber, 1969; Rawitch et al., 1969). The optical and fluorescence spectral properties of pyrene–PFn (Figure 2) were indistinguishable from those of other 1-pyrenebutyrate-conjugated proteins (Knopp & Weber, 1969; Rawitch et al., 1969). Preparations of pyrene–PFn utilized in this study contained 0.3–0.8 mol of pyrenebutyrate/mol of PFn. Under these conditions, pyrene–PFn bound to gelatin–Sepharose and heparin–Sepharose columns with affinities comparable to that of the underivatized starting material (data not shown). We also observed that the thrombin and cathepsin D proteolytic digestion pattern of pyrene–PFn was identical with that of native PFn (data not shown). All PFn fragments isolated from these digests exhibited fluorescence emission spectra characteristic of bound pyrenebutyrate (data not shown). This confirmed that labeling was not confined to any specific region of the PFn subunit. We also observed that the $s_{20,w}$ value (12.8 S) and far-UV CD spectrum of pyrene–PFn were indistinguishable from those of native PFn (data not shown). The ~30× higher fluorescence quantum yield exhibited by pyrenebutyrate relative to dansylcadaverine and the facile preparation of milligram quantities of pyrene–PFn by the nonenzymatic labeling procedure employed here facilitated detailed spectroscopic study of this PFn derivative.

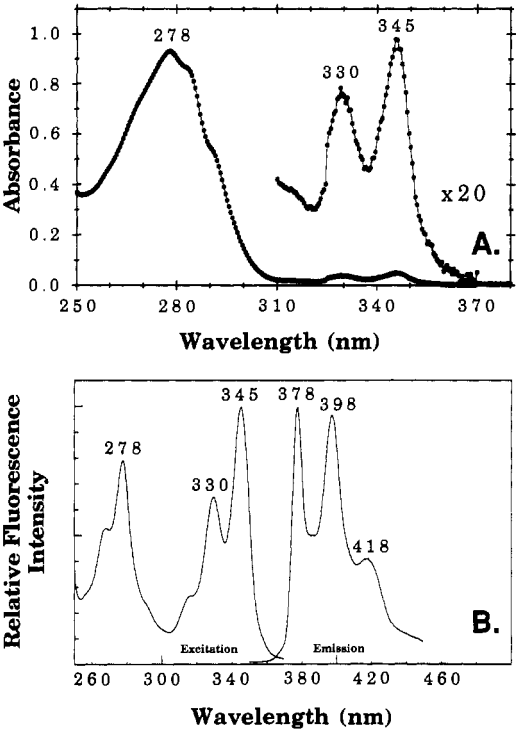

FIGURE 2: Characteristic absorption (A) and fluorescence (B) spectra exhibited by pyrene–PFn preparations in PBS. The excitation and emission wavelengths used to generate the fluorescence data were 330 and 398 nm, respectively.

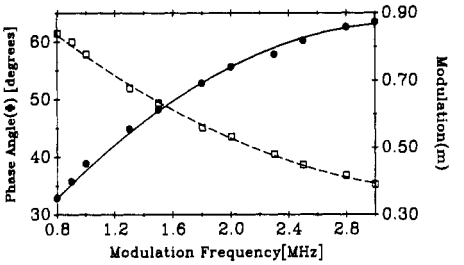

FIGURE 3: Phase angle (circles) and modulation (squares) data obtained for pyrene–PFn at 20 °C in PBS. Phase shift (—) and demodulation (---) predicted for doubly exponential fluorescence decay with components $\tau_1 = 34$ ns and $\tau_2 = 134$ ns representing 7% and 93% of the total emission intensity, respectively.

Pyrene–PFn Fluorescence Lifetime Measurements. Phase shift and demodulation measurements of pyrene–PFn at 20 °C yielded data that could be fit confidently to a model assuming doubly exponential fluorescence decay with components $\tau_1 = 34$ ns and $\tau_2 = 134$ ns representing 7% and 93% of the observed emission intensity, respectively (Figure 3). The complexity of the fluorescence decay dictated the use of the second-order average lifetime, $\langle\tau\rangle$, in subsequent ρ_H calculations. We noticed that pyrene–PFn fluorescence intensity decreased markedly as temperature was increased (Figure 4, inset). Since changes in relative fluorescence intensity often mirror changes in fluorescence lifetime, we examined the relationship by which $\langle\tau\rangle$ varied as a function of temperature (Figure 4). As would be expected, $\langle\tau\rangle$ decreased in a linear fashion as temperature was increased.

Rotational Relaxation Measurements on Pyrene–PFn. The biphasic nature of the pyrene–PFn isothermal (20 °C) depolarization curve became evident when we extended our po-

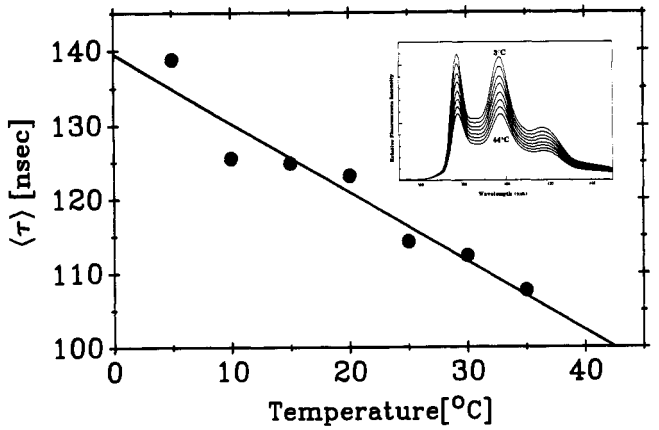

FIGURE 4: Effect of temperature on the pyrene–PFn second-order average fluorescence lifetime. (Inset) The traces shown from top to bottom correspond to pyrene–PFn emission spectra obtained at 3, 9, 15, 20, 26, 31, 38, and 44 °C, respectively.

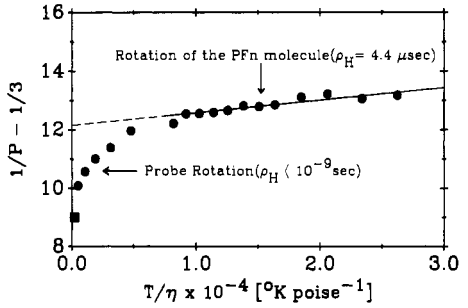

FIGURE 5: (Circles) Perrin plot obtained by measuring pyrene–PFn fluorescence polarization as a function of sucrose concentration [0–55% (w/v)] at 20 °C in PBS. (Square) An estimate of $(1/P_0 - 1/3)$ derived from a polarization measurement in 55% sucrose at 4 °C.

larization measurements to solutions of high viscosity (Figure 5). The depolarization observed at low viscosity ($T/\eta > 8000$ K P^{-1}; i.e., ≤30% sucrose) arises from slow overall rotation of the PFn molecule while the high-viscosity component ($T/\eta < 5000$ K P^{-1}; i.e., ≥40% sucrose) emanates from the rapid localized rotational motion of the fluorescent probe. Similar to the observations made above (Figure 1A, squares) for dansylcadaverine–PFn, the slope associated with the low-viscosity component of the isothermal Perrin plot (Figure 1B, squares) was small compared to that of the nonisothermal depolarization curve (Figure 1B, circles). We also observed the apparent increase in ρ_H when the nonisothermal experiment was carried out in buffer containing 35% sucrose (Figure 1B, triangles).

However, unlike dansylcadaverine–PFn, we detected a small but significant depolarization associated with the slow overall rotation of the dimeric PFn molecule (Figure 1B, squares). We note that this small depolarization ($\Delta P = 0.004$) required that we "correct" for the additional polarization contributed by sucrose (~0.001) in our data analysis. The ρ_H calculated from these data (4.4 ± 0.9 μs) is 7 (±1.4) times longer than that predicted for a 520-kDa sphere containing 0.4 g of H_2O/g of protein ($\rho_0 = 0.63$ μs). The simplest hydrodynamic model which fits the data is an oblate ellipsoid with an axial ratio of 15:1 (Figure 6). All prolate models can unambiguously be excluded by this result (Figure 6). We estimate that the disk-shaped PFn molecule has a diameter and thickness of 30 and 2.0 nm, respectively.

Analysis of the polarization data obtained for the 1-pyrenebutyrate conjugate of the thrombin-derived 190/170-kDa PFn fragment (Figure 7; circles) assumed that this PFn derivative had the same fluorescence lifetime as pyrene–PFn.

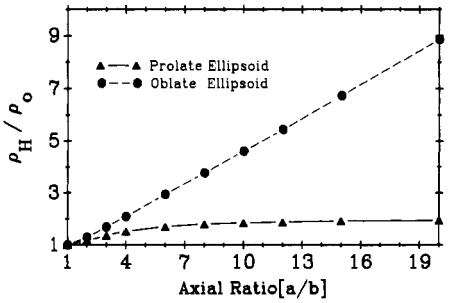

FIGURE 6: Mean harmonic rotational relaxation times expected for various prolate (triangles) and oblate (circles) ellipsoidal models. The derivation of the functions relating the ρ_H/ρ_0 ratio to ellipticity is outlined in the Appendix.

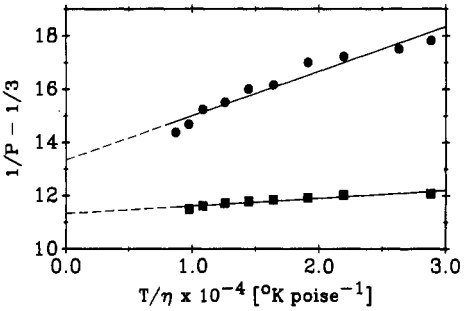

FIGURE 7: (Circles) Pyrene–190/170-kDa PFn fragment depolarization curve generated under isothermal conditions. The ρ_H calculated from these data is 0.92 ± 0.11 μs. (Squares) Pyrene–PFn data shown for comparison (ρ_H = 4.4 ± 0.9 μs). In these experiments, the temperature to solvent viscosity ratio was varied by the addition of sucrose (0–30%) at 20 °C. PBS was the solvent.

Since we established that the relative quantum yields of pyrene–PFn and pyrene–190/170-kDa PFn fragment fluorescence were identical (data not shown), this assumption appeared to be valid. Pyrene–190/170-kDa PFn fragment, which retained full PFn heparin and gelatin binding activity (data not shown), exhibited a much faster rotational relaxation rate (ρ_H = 0.92 ± 0.11 μs) than pyrene–PFn (Figure 7, squares; ρ_H = 4.4 ± 0.9 μs). Taken together with its observed $s_{20,w}$ near 6 S (Benecky et al., 1988a), we conclude that the 190/170-kDa PFn fragment is monomeric under physiologic buffer conditions. The 190/170-kDa PFn fragment ρ_H value is approximately 4–5 times longer than that predicted for an equivalent hydrated sphere ρ_0 = 0.22 μs. This indicates that this peptide, like native PFn, has an oblate shape under physiologic buffer conditions (Figure 6). We also observed that the far-UV CD spectrum of the 190/170-kDa PFn fragment was superimposable upon that of the PFn/amino-terminal 29-kDa PFn fragment CD difference spectrum (data not shown).

Previous investigators have noted curvature in Perrin plots derived from experiments in which dansylcadaverine–PFn (Williams et al., 1982) and ANS–PFn (Ingham et al., 1988) fluorescence polarization was monitored as a function of temperature. Dramatic temperature-dependent changes in the electron spin resonance spectrum of a maleimide spin-labeled PFn preparation have also been reported (Lai & Tooney, 1984). These observations have been taken as supporting evidence for temperature-induced PFn conformational changes between 0 and 40 °C. Since we believed that the temperature-dependent effects noted above were merely manifestations of "thermally activated" probe rotation, we investigated whether temperature-induced changes in PFn conformation could occur by studying the temperature dependence of the PFn ρ_H value (Figure 8). The 10, 20, and 30 °C pyrene–PFn isothermal depolarization curves yielded a family of lines that

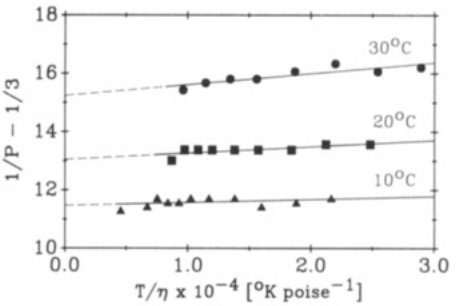

FIGURE 8: Comparison of pyrene–PFn isothermal depolarization curves at 10 °C (triangles), 20 °C (squares), and 30 °C (circles), respectively. Other experimental conditions same as in Figure 7. The high-viscosity data (i.e., $T/\eta < 5000$ K P^{-1}), which show nonlinearity due to the rapid independent rotational motion of the fluorescent probe, have been omitted for clarity.

were approximately parallel. This indicated that ρ_H did not change significantly within this temperature range. From these data (using eq 5), we also estimated that the thermodynamic barrier to free rotation of the 1-pyrenebutyrate probe was small (~2 kcal/mol).

Electron Microscopy of PFn. Electron micrographs of negatively stained PFn specimens on carbon showed rounded compact structures with diameters around 20 nm (Figure 9A,B). Structures of similar shape and dimensions have been noted in STEM images of PFn that had been freeze-dried on carbon (Tooney et al., 1983). However, PFn specimens that had been sprayed onto carbon in the presence of 30% glycerol and visualized by platinum rotary-shadowing appeared as extended strandlike structures (Figure 9C). The dimensions of these extended structures (140 × 2 nm), which are similar to those previously reported for rotary-shadowed PFn specimens on mica (Engel et al., 1981; Erickson et al., 1981), seemed incompatible with the PFn structural model derived from our pyrene–PFn fluorescence polarization measurements.

Discussion

Implicit in our analysis of the fluorescence polarization data is the assumption that two mutually independent dynamic processes depolarize the fluorescence exhibited by the dansylcadaverine and 1-pyrenebutyrate conjugates of PFn: rapid (subnanosecond) localized rotational motion of the fluorescent probe and slow (ρ_H = 4.4 μs) global rotation of the dimeric PFn molecule. Since the former process is temperature dependent (Wahl & Weber, 1967; Weltman & Edelman, 1967), isothermal polarization measurements have been employed in this study to estimate the rotational relaxation time of PFn and the thrombin-derived 190/170-kDa PFn fragment under physiologic buffer conditions. We estimated ρ_H from the low-viscosity component (i.e. $T/\eta > 8000$ K P^{-1}; ≤30% sucrose at 20 °C) of the pyrene–PFn isothermal Perrin plot. This procedure assumes that the localized and global rotational motions of the probe and protein respectively are temporally distinguishable. This condition is fulfilled when $3\tau/\rho_c \gg 1$ (Weber, 1953), where ρ_c is the rotation relaxation time of the protein side chain bearing the fluorescent probe. Since τ = 123 ns (Figure 3) and $\rho_c \sim 0.2$ ns (Wahl & Weber, 1967), this assumption appears valid ($3\tau/\rho_c \approx 1800$). We also made the assumption based on the linearity of the low-viscosity component of the isothermal Perrin plot that moderate levels of sucrose [i.e., ≤30% (w/v)] do not perturb the native structure of the PFn molecule.

Keeping in mind the assumptions made above, the ρ_H calculated from polarization measurements made on pyrene–PFn under isothermal conditions is approximately 7 times longer (4.4 ± 0.9 μs) than that predicted for an equivalent hydrated sphere (ρ_0 = 0.63 μs). This result, which rigorously excludes all possible prolate ellipsoidal models, indicates that the dimeric PFn molecule has a rigid oblate shape under physiologic buffer conditions. We estimate that the disk-shaped PFn molecule has a diameter and thickness of 30 and 2.0 nm, respectively. This model is in good agreement with the PFn structure predicted by small-angle X-ray and neutron scattering measurements (Sjöberg et al., 1987). This structural model also appears consistent with the "compact" structures observed during electron microscopic examination of negatively stained (Figure 9A,B) and freeze-dried (Tooney et al., 1983) PFn specimens deposited on carbon. We note, however, that the dimensions of the PFn molecule obtained by electron microscopy were somewhat smaller (~20 nm) than those

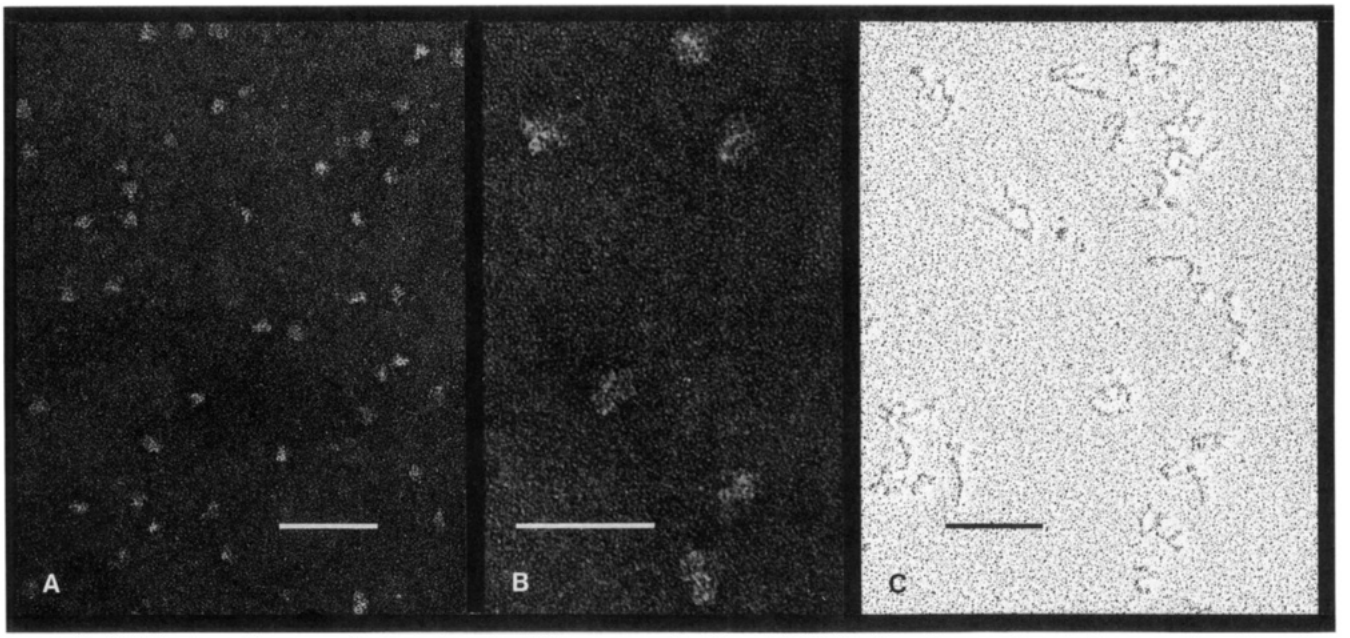

FIGURE 9: (A) Electron microscopy of negatively stained PFn at a magnification of 128700×. Samples were deposited upon an ultrathin carbon film (25–30 Å in thickness) and visualized by negative staining with 2% uranyl acetate. Bar = 100 nm. (B) Same as (A) except at a magnification of 363800×. Bar = 50 nm. (C) Electron microscopy of rotary-shadowed PFn at a magnification of 128700×. Samples were sprayed onto a carbon film in the presence of 30% (v/v) glycerol and visualized by platinum rotary-shadowing. Bar = 100 nm.

predicted by fluorescence polarization (~30 nm). This could reflect partial dehydration of the molecule during specimen preparation for electron microscopy.

Our fluorescence data exclude models which represent the solution structure of PFn under physiologic conditions as an extended molecule (Engel et al., 1981; Erickson et al., 1981). Previous work has shown that glycerol induces a change in PFn conformation under physiologic buffer conditions (Rocco et al., 1983). Therefore, we believe that the extended structures observed during electron microscopic examination of rotary shadowed PFn specimens (Engel et al., 1981; Erickson et al., 1981; Erickson & Carrell, 1983; Figure 9c) largely reflect a PFn conformational change induced by glycerol exposure during specimen preparation. However, we cannot exclude the possibility that an electrostatic interaction between PFn and the substrate (e.g., mica) could also participate in this effect (Tooney et al, 1983).

Models which invoke extensive segmental flexibility of the PFn peptide backbone under physiologic buffer conditions (Williams et al., 1982; Lai & Tooney, 1984; Lai et al., 1984; Forastieri & Ingham, 1985; Narasimhan & Lai, 1989) can also be excluded by our fluorescence polarization data. Our data indicate that the rapid "thermally activated" rotational motion of the fluorescent probe (Weber, 1952), rather than PFn segmental flexibility, gives rise to the shorter than expected ρ_H values previously calculated from the PFn (Williams et al., 1982) and the gelatin binding 42-kDa PFn fragment (Forastieri & Ingham, 1985) nonisothermal polarization data. Since the PFn rotational relaxation times estimated from ESR measurements by Lai and co-workers (Lai & Tooney, 1984; Lai et al., 1984; Narasimhan & Lai, 1989) are also approximately 2 orders of magnitude shorter than our fluorescence polarization derived value (ρ_H = 4.4 μs), we predict that the rapid independent rotational motion of the maleimide spin-label contributes significantly to the observed ESR signal. Spin-labeled maleimide covalently bound to the ADP/ATP carrier has been shown to be an unsuitable probe of protein rotational diffusion because of its indepedent rotational motion (Horváth et al., 1989); this observation establishes precedence for our contention. We also note that the ESR-derived rotational relaxation time decreased progressively at higher sample temperatures (Lai & Tooney, 1984). This behavior is quite reminiscent of the "thermally-activated" depolarization noted in the present study. Furthermore, our parallel observation of dramatic changes in both sedimentation velocity 13 S → 6 S and ρ_H (4.4 μs → 0.92 μs) between PFn and thrombin-derived 190/170-kDa PFn fragment indicates that our fluorescence polarization derived ρ_H is a parameter sensitive to changes in the hydrodynamic characteristics of the PFn molecule. In contrast, the ESR hyperfine splitting appeared to be insensitive to the size differences between PFn and the trypsin-derived 215-, 185-, 75-, and 31-kDa PFn fragments (Narasimhan & Lai, 1989). Therefore, we believe that the ESR measurements of Lai and co-workers are essentially monitoring the independent rotational motion of the PFn sulfhydryl groups which bear the maleimide spin-label. Consequently, we must question the validity of the ESR evidence supporting PFn conformational changes induced by temperature (Lai & Tooney, 1984) or adsorption to a solid substrate (Narasimhan & Lai, 1989).

We found that the Perrin plots obtained isothermally at 10, 20, and 30 °C respectively yielded a family of approximately parallel lines (Figure 8). This observation suggests that ρ_H does not change significantly throughout this temperature interval. Therefore, we find no evidence for the temperature-induced changes in PFn conformation reported previously (Williams et al., 1982; Lai & Tooney, 1984; Ingham et al., 1988). We believe that the temperature-dependent spectral changes noted in these studies are simple manifestations of "thermally-activated" probe rotation.

The observed ρ_H for the thrombin-derived 190/170-kDa PFn fragment (0.92 ± 0.11 μs), which is 4–5 times longer than that predicted for an equivalent hydrated sphere (ρ_0 = 0.22 μs), indicates that this peptide retains the disk-like structure characteristic of the native molecule. We estimate that the 190/170-kDa PFn fragment has a diameter and thickness of 18 and 1.9 nm, respectively. We also observed that the far-UV CD spectrum of the 190/170-kDa PFn fragment was superimposable upon that of the PFn/amino-terminal 29-kDa PFn fragment CD difference spectrum. Therefore, PFn and the 190/170-kDa PFn fragment must be very similar in their secondary and tertiary structural characteristics. We can also conclude that the 30-kDa amino-terminal domain does not play an essential role in the structural stabilization of an isolated PFn subunit.

Since the analysis of PFn fluorescence polarization data using Perrin analysis has generally been misapplied in the literature, we outline the factors that should be considered when this approach is used in the future (Weber, 1953). Perrin plots constructed from polarization measurements made as a function of temperature often yield anomalously short ρ_H values due to "thermally-activated" depolarization arising from the localized rotational motion of the protein side chains bearing the fluorescent probe. This temperature-dependent process can be diagnosed rather simply by comparing the y intercepts of Perrin plots generated under nonisothermal and isothermal conditions, respectively. Probe rotation would cause the isothermal value to be significantly larger than the nonisothermal value. The nonisothermal approach would also not be valid in our present system due to the fact that the pyrene–PFn fluorescence lifetime is temperature dependent. It is also critical to choose a fluorescent probe with a lifetime comparable to the time scale of the rotational motion under investigation. For example, the slow global rotational motion of the PFn molecule ($\rho_H = 4.4 \times 10^{-6}$ s) is insensitive to short lifetime fluorescent probes such as fluorescein ($\tau = 4.5 \times 10^{-9}$ s) and dansylcadaverine ($\tau = 1.2 \times 10^{-8}$ s). These probes would be biased toward the detection of the rotational motion of the side chains bearing the fluorescent probe ($\rho_c = 2.0 \times 10^{-10}$ s). For this reason, we employed the long-lifetime probe 1-pyrenebutyrate ($\tau = 1.2 \times 10^{-7}$ s) in our experimental system. If a longer fluorescent lifetime probe were available, the PFn ρ_H value could be determined with greater accuracy.

Acknowledgments

We thank the Mout Sinai Medical Center Foundation for the funds which allowed us to purchase the SLM–Amino SPF500C spectrofluorometer. We are grateful to Drs. Kevin Siebenlist (Sinai Samaritan Medical Center, Milwaukee, WI) and John Fenton (New York State Department of Health, Albany, NY) for providing us with factor XIII and thrombin, respectively. We acknowledge the assistance provided by Dr. James Mattheis and John Catlo (SLM–Amino, Inc., Urbana, IL) during the pyrene–PFn fluorescence lifetime measurements. We thank Angela Mallett for secretarial support and William Semrad for photographic services.

Appendix

Rotational Relaxation Times Expected for Various Hydrodynamic Models. (A) Sphere. ρ_0, the rotational relaxation time expected if PFn were spherical, was estimated by using

eq 6. Substituting $R = 8.314 \times 10^7$ erg mol^{-1} K^{-1}, $T = 298$ K, $\eta = 0.0089$ P, and $V = 5.82 \times 10^5$ cm^3 mol^{-1} into this equation, we obtained $\rho_0 = 6.28 \times 10^{-7}$ s. This calculation assumed that PFn had a molecular weight of 520K, a partial specific volume of 0.72 mL/g (Mosesson et al., 1975), and a hydration of 0.40 g of H_2O/g of protein (Rocco et al., 1987). Using an average molecular weight of 180K and making similar assumptions for partial specific volume and hydration, we estimated $\rho_0 = 2.17 \times 10^{-7}$ s for the thrombin-derived 190/170-kDa PFn fragment.

$$\rho_0 = 3\eta V/RT \tag{6}$$

(*B*) *Elliptical Models.* The disk-shaped oblate ellipsoid is characterized by a single short semiaxis, b, and two identical long semiaxes, a. The cigar-shaped prolate ellipsoid is characterized by a single long semiaxis, a, and two identical short semiaxes, b. For each type of ellipsoid, the axial ratio (p_r) is defined as a/b, the ratio of the long to the short semiaxes. Two rotational frictional coefficients characterize an ellipsoid: f_a for rotation about the a semiaxis, and f_b for rotation about the b semiaxis. Expressions for these frictional coefficients have been given by Cantor and Schimmel (1980). These frictional coefficients are defined relative to f_0, the rotational frictional coefficient of a hydrated sphere of equivalent volume:

$$F_a = f_a/f_0 = 4(1 - p^2)/3(2 - p^2S) \tag{7a}$$

$$F_b = f_b/f_0 = 4(1 - p^4)/3p^2[S(2 - p^2) - 2] \tag{7b}$$

In these equations, S and p are defined in the following way:

prolate ellipsoid

$$S = 2(1 - p^2)^{-1/2} \ln \{[1 + (1 - p^2)]^{1/2}/p\} \tag{8a}$$

$$p = b/a = 1/p_r \tag{8b}$$

oblate ellipsoid

$$S = 2(p^2 - 1)^{-1/2} \tan^{-1} (p^2 - 1)^{1/2} \tag{9a}$$

$$p = a/b = p_r \tag{9b}$$

When these expressions are evaluated, it is found that oblate ellipsoids produce approximately the same friction, whether they rotate about the long axis (f_a) or the short axis (f_b). Both motions involved more friction than does the rotation of an equivalent sphere. Prolate ellipsoids rotate around their long axis (f_a) with less friction than that of an equivalent hydrated sphere. However, rotation about its short axis (f_b) is accompanied by extremely great friction.

Each rotational frictional coefficient can be related to a rotational relaxation time, ρ, which measures the rate at which an anisotropic distribution relaxes to equilibrium through a particular rotational motion. For ellipsoids relative to equivalent hydrated spheres:

prolate ellipsoid

$$\rho_a/\rho_0 = F_b \tag{10a}$$

$$\rho_b/\rho_0 = 2F_aF_b/(F_a + F_b) \tag{10b}$$

oblate ellipsoid

$$\rho_b/\rho_0 = F_a \tag{11a}$$

$$\rho_a/\rho_0 = 2F_aF_b/(F_a + F_b) \tag{11b}$$

However, steady-state fluorescence polarization measurements yield ρ_H, the harmonic mean of ρ_a and ρ_b. This quantity is calculated for prolate and oblate ellipsoids by using eq 12 and 13, respectively.

prolate ellipsoid

$$\rho_H^{-1} = 1/3[\rho_a^{-1} + 2(\rho_b)^{-1}] \tag{12}$$

oblate ellipsoid

$$\rho_H^{-1} = 1/3[2(\rho_a)^{-1} + \rho_b^{-1}] \tag{13}$$

Therefore, we can obtain functions relating ρ_H/ρ_0 to ellipticity (Figure 6) by using the following three-step method: (1) evaluating F_a and F_b for a given axial ratio (eq 7–9); (2) utilizing F_a and F_b to calculate ρ_a and ρ_b (eq 10 and 11); (3) computing the harmonic mean (ρ_H) of ρ_a and ρ_b (eq 12 and 13).

Estimation of PFn Size. The volume of an oblate ellipsoid, V, equals $(4/3)\pi a^2 b$. Using $V = 9.66 \times 10^{-19}$ cm^3/molecule and the axial ratio ($a/b = 15$) predicted by fluorescence polarization, we estimated the diameter ($2a$) and thickness ($2b$) of the disk-shaped PFn molecule to be 30 and 2 nm, respectively.

References

Acuña, A. U., Gonzalez-Rodriguez, J., Lillo, M. P., & Naqvi, K. R. (1987) *Biophys. Chem. 26*, 63–70.

Balian, G., Click, E. M., Crouch, E., Davison, J. M., & Bornstein, P. (1979) *J. Biol. Chem. 254*, 1429–1432.

Benecky, M. J., Kolvenbach, C. G., Amrani, D. L., & Mosesson, M. W. (1988a) *Biochemistry 27*, 7565–7571.

Benecky, M. J., Kolvenbach, C. G., & Mosesson, M. W. (1988b) *J. Cell Biol. 107*, 409a.

Brochon, J.-C., & Wahl, P. (1972) *Eur. J. Biochem. 25*, 20–32.

Cantor, C. R., & Schimmel, P. R. (1980) in *Biophysical Chemistry*, Part II, pp 562–563, W. H. Freeman, San Francisco, CA.

Chen, A. B., Amrani, D. L., & Mosesson, M. W. (1977) *Biochim. Biophys. Acta 493*, 310–322.

Engel, J., Odermatt, E., Engel, A., Madri, J., Furthmayr, H., Rohde, H., & Timpl, R. (1981) *J. Mol. Biol. 157*, 97–120.

Engvall, E., & Ruoslahti, E. (1977) *Int. J. Cancer 20*, 1–5.

Erickson, H. P., & Carrell, N. A. (1983) *J. Biol. Chem. 258*, 14539–14544.

Erickson, H., Carrell, N., & McDonagh, J. (1981) *J. Cell Biol. 91*, 673–678.

Forastieri, H., & Ingham, K. C. (1985) *J. Biol. Chem. 260*, 10546–10550.

Hermans, J. (1985) in *Plasma Fibronectin Structure and Function* (McDonagh, J., Ed.) pp 53–75, Marcel Dekker, New York.

Homandberg, G. A., & Erickson, J. W. (1986) *Biochemistry 25*, 6917–6725.

Homandberg, G. A., Amrani, D. L., Evans, D. B., Kane, C. M., Ankel, E., & Mosesson, M. W. (1985) *Arch. Biochem. Biophys. 238*, 652–663.

Horváth, L. I., Munding, A., Beyer, K., Klingenberg, M., & Marsh, D. (1989) *Biochemistry 28*, 407–414.

Ingham, K. C., Brew, S. A., & Isaacs, B. S. (1988) *J. Biol. Chem. 263*, 4624–4628.

Knopp, J. A., & Weber, G. (1969) *J. Biol. Chem. 244*, 6309–6315.

Kornblihtt, A. R., Umezawa, K., Vibe-Pedersen, K., & Baralle, F. E. (1985) *EMBO J. 4*, 1755–1759.

Koteliansky, V. E., Bejanian, M. V., & Smirnov, V. N. (1980) *FEBS Lett. 120*, 283–288.

Laemmli, U. K. (1970) *Nature (London) 22*, 680–685.

Lai, C.-S., & Tooney, N. M. (1984) *Arch. Biochem. Biophys. 228*, 465–473.

Lai, C.-S., Tooney, N. M., & Ankel, E. G. (1984) *Biochemistry 23*, 6393–6397.
Lakowicz, J. R. (1983a) *Principles of Fluorescence Spectroscopy*, pp 75–91, Plenum, New York.
Lakowicz, J. R. (1983b) *Principles* of *Fluorescence Spectroscopy*, pp 126–128, Plenum, New York.
Lorand, L., & Gotoh, T. (1970) *Methods Enzymol. 19*, 770–782.
March, J. C., Parikh, I., & Cuatrecasas, P. (1974) *Anal. Biochem. 60*, 149–152.
Miekka, S. I., Ingham, K. C., & Menache, D. (1982) *Thromb. Res. 27*, 1–14.
Mosesson, M. W., & Umfleet, R. A. (1970) *J. Biol. Chem. 245*, 5728–5736.
Mosesson, M. W., Chen, A. B., & Huseby, R. M. (1975) *Biochim. Biophys. Acta 386*, 509–524.
Narasimhan, C., & Lai, C.-S. (1989) *Biochemistry 28*, 5041–5046.
Odermatt, E., & Engel, J. (1989) in *Fibronectin* (Mosher, D. F., Ed.) pp 25–43, Academic Press, San Diego, CA.
Odermatt, E., Engel, J., Richter, H., & Hörmann, H. (1982) *J. Mol. Biol. 159*, 109–123.
Perrin, F. (1934) *J. Phys. 5*, 497–511.
Price, T. M., Rudee, M. L., Pierschbacher, M., & Ruoslahti, E. (1982) *Eur. J. Biochem. 129*, 359–363.
Provencher, S. W., & Glöckner, J. (1981) *Biochemistry 20*, 33–37.
Rawitch, A. B., Hudson, E., & Weber, G. (1969) *J. Biol. Chem. 244*, 6543–6547.
Rocco, M., Carson, M., Hantgan, R., McDonagh, J., & Hermans, J. (1983) *J. Biol. Chem. 258*, 14545–14549.
Rocco, M., Infusini, E., Daga, M. G., Gogioso, L., & Cuniberti, C. (1987) *EMBO J. 6*, 2343–2349.
Sjöberg, B., Pap, S., Österlund, E., Österlund, K., Vuento, M., & Kjems, J. (1987) *Arch. Biochem. Biophys. 255*, 347–353.
Smith, R. L., & Griffin, C. A. (1985) *Thromb. Res. 37*, 91–101.
Sober, H. A., Ed. (1970) *CRC Handbook of Biochemistry*, 2nd ed., pp J288–J291, Chemical Rubber Co., Cleveland, OH.
Tooney, N. M., Mosesson, M. W., Amrani, D. L., Hainfeld, J. F., & Wall, J. S. (1983) *J. Cell Biol. 97*, 1686–1692.
Wahl, P., & Weber, G. (1967) *J. Mol. Biol. 30*, 371–382.
Wall, J. S., Hainfeld, J. F., & Chung, K. D. (1985) in *Proceedings of the 43rd Annual Meeting of the Electron Microscopy Society of America* (Bailey, G. W., Ed.) pp 716–717, San Francisco Press, San Francisco, CA.
Weast, R. C., Ed. (1972) *CRC Handbook of Chemistry and Physics*, 53rd ed., F36, Chemical Rubber Co., Cleveland, OH.
Weber, G. (1952) *Biochem. J. 51*, 145–154.
Weber, G. (1953) *Adv. Protein Chem. 8*, 415–459.
Weber, G. (1981) *J. Phys. Chem. 85*, 949–953.
Weltman, J. K., & Edelman, G. M. (1967) *Biochemistry 6*, 1437–1447.
Williams, E. C., Janmey, P. A., Ferry, J. D., & Mosher, D. F. (1982) *J. Biol. Chem. 257*, 14973–14978.

Mechanism of Inhibition of the (Ca^{2+}–Mg^{2+})-ATPase by Nonylphenol†

F. Michelangeli,‡ S. Orlowski,§ P. Champeil,§ J. M. East,‡ and A. G. Lee*,‡
Department of Biochemistry, University of Southampton, Southampton SO9 3TU, U.K., and SBPH/DB and URA CNRS D1290, CEN Saclay, 91191 Gif-sur-Yvette Cedex, France

Received July 14, 1989; Revised Manuscript Received November 16, 1989

ABSTRACT: The effects of nonylphenol and 3,5-dibutyl-4-hydroxytoluene (BHT) on the activity of the (Ca^{2+}–Mg^{2+})-ATPase of skeletal muscle sarcoplasmic reticulum have been studied. At high concentrations, both inhibit the ATPase activity of the ATPase either in native lipid or in bilayers of dioleoylphosphatidylcholine but, at low concentrations, an increase in ATPase activity is observed, particularly for the ATPase reconstituted into dimyristoleoylphosphatidylcholine. Neither nonylphenol nor BHT binds at the lipid–protein interface of the ATPase. Nonylphenol decreases the effective equilibrium constant for phosphorylation of the ATPase by P_i probably through an increase in the effective rate of dephosphorylation of the phosphorylated ATPase. It also decreases the effective rate of the E2–Ca_2E1 transition and increases the effective equilibrium constant E2/E1 for the ATPase. Inhibition of ATPase activity follows from the slowing of the E2–E1 transition despite increases in effective rates for dephosphorylation and for the transport step, Ca_2E1P–E2P. Since nonylphenol has been shown to affect equilibrium constants for various steps in the reaction pathway of the ATPase, inhibition of activity of the ATPase cannot follow from effects on the fluidity (viscosity) of the membrane, since fluidity alone cannot affect equilibrium properties of the system.

The activities of many membrane proteins have been found to be affected by a wide range of hydrophobic molecules. Although some of these effects may arise from specific interactions between the hydrophobic additive and a distinct site on the protein, the majority of the effects are likely to be nonspecific. Since hydrophobic molecules partition extensively into the phospholipid component of biological membranes, effects of such molecules could follow from an effect on the fluidity of the bilayer, with the activity of membrane proteins being very sensitive to the fluidity, or viscosity, of the surrounding lipid (Sinensky, 1974; Chong et al., 1985; Almeida et al., 1986). To test this possibility, we previously studied the effect of lipid fluidity on the activity of the (Ca^{2+}–Mg^{2+})-ATPase purified from the sarcoplasmic reticulum of

† The SERC are thanked for financial support.
‡ University of Southampton.
§ SEN Saclay.

0006-2960/90/0429-3091$02.50/0